ACS chemical biology

Letters

pubs.acs.org/acschemicalbiology

Structure, Biochemistry, and Inhibition of Essential 4′-Phosphopantetheinyl Transferases from Two Species of *Mycobacteria*

Christopher R. Vickery,[†,§] Nicolas M. Kosa,[†] Ellen P. Casavant,[†] Shiteng Duan,[†] Joseph P. Noel,*[,‡,§] and Michael D. Burkart*[,†]

[†]Department of Chemistry and Biochemistry, University of California, San Diego, 9500 Gilman Drive, La Jolla, California 92093-0358, United States

[‡]Howard Hughes Medical Institute, 10010 N. Torrey Pines Road, La Jolla, California 92037, United States

[§]Jack Skirball Center for Chemical Biology and Proteomics, The Salk Institute, 10010 N. Torrey Pines Road, La Jolla, California 92037, United States

Supporting Information

ABSTRACT: 4′-Phosphopantetheinyl transferases (PPTase) post-translationally modify carrier proteins with a phosphopantetheine moiety, an essential reaction in all three domains of life. In the bacterial genus *Mycobacteria*, the Sfp-type PPTase activates pathways necessary for the biosynthesis of cell wall components and small molecule virulence factors. We solved the X-ray crystal structures and biochemically characterized the Sfp-type PPTases from two of the most prevalent Mycobacterial pathogens, PptT of *M. tuberculosis* and MuPPT of *M. ulcerans*. Structural analyses reveal significant differences in cofactor binding and active site composition when compared to previously characterized Sfp-type PPTases. Functional analyses including the efficacy of Sfp-type PPTase-specific inhibitors also suggest that the Mycobacterial Sfp-type PPTases can serve as therapeutic targets against Mycobacterial infections.

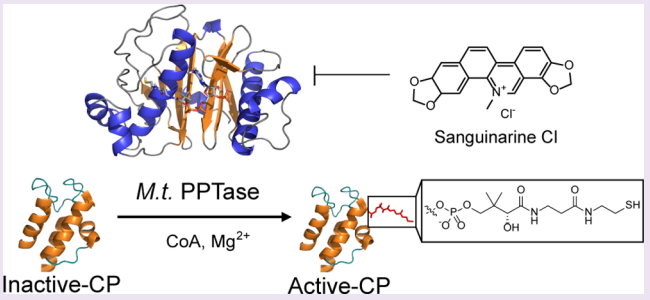

Widespread sickness throughout the world is caused by the pathogenic bacterial genus *Mycobacterium*.[1] Although antibiotic regimes for mycobacterial infections have been in place for decades, emerging resistance to current antibiotics strains existing resources and necessitates ongoing development of new treatment strategies.[2] Two of the most prominent pathogenic mycobacterial species are *M. tuberculosis*, the causative agent of tuberculosis,[3] and *M. ulcerans*, responsible for Buruli ulcer.[4] Mycobacteria possess a complex and robust cell wall composed of uncommon fatty acids, glycolipids, and polyketide natural products that enable infection and immune evasion.[5,6] Small molecule virulence factors include mycobactin,[7] a peptidic siderophore found in all mycobacteria that facilitates iron acquisition from hosts required for normal growth,[8] and the small molecule mycolactone,[9] a plasmid-encoded polyketide toxin produced by M. *ulcerans*.

Biosyntheses of these cell wall components and small molecule virulence factors require large multidomain synthases containing carrier protein (CP) domains. CPs tether the elongating product through a thioester linkage to a post-translationally attached 4′-phosphopantetheinyl group.[10,11] Post-translational modifications are carried out by Mg^{2+}-dependent 4′-phosphopantetheinyl transferases (PPTases).[12] PPTases attach the 4′-phosphopantetheine arm of coenzyme A (CoA) to a conserved serine residue of the CP (Supplementary Figure 1). The terminal thiol of the CP-bound phosphopantetheine serves as a tether for the nascent product as it visits each catalytic domain for elongation and tailoring. Many bacteria contain two types of PPTases: the acyl carrier protein synthase (AcpS) and a secondary PPTase named for the *Bacillus subtilis* PPTase associated with surfactin biosynthesis (Sfp).[13] AcpS-type PPTases activate acyl CPs associated with fatty acid synthases (FAS),[14,15] while Sfp-type PPTases modify CPs involved in the production of secondary metabolites, including polyketide synthases (PKS), hybrid FAS/PKS, and non-ribosomal peptide synthases (NRPS).[12] A single Sfp-type PPTase in *Homo sapiens* called aminoadipate semialdehyde dehydrogenase phosphopantetheinyl transferase (HsPPT) activates FAS-mediated biosynthesis,[16] lysine metabolism,[17] and tetrahydrofolate biosynthesis.[18] The structure of the AcpS-type PPTase from *M. tuberculosis* has been solved;[19,20] however, there are currently no structures of the Sfp-type PPTase from *M. tuberculosis*, PptT. To date, only two Sfp-type PPTases have

Received: April 8, 2014
Accepted: June 25, 2014
Published: June 25, 2014

been structurally characterized: Sfp of *B. subtilis*[21,22] and HsPPT of *H. sapiens*.[16]

Sfp-type PPTase genetic knockouts in *Mycobacterium smegmatis* and *Mycobacterium bovis* previously showed that each of these PPTases are essential gene products for cell growth.[23] More importantly, generation of a *M. tuberculosis* strain with an inducible PptT expression cassette resulted in elimination of cell viability without PptT expression and a reduced bacterial load in mice infected with the mutant *M. tuberculosis* strain compared to wild type strains.[24] Due to its important role in multiple aspects of mycobacterial secondary metabolism and concomitant bacterial viability, discovery of specific inhibitors of this enzyme will enable new therapeutic leads for the treatment of mycobacterial infections. We solved the 3D X-ray crystallographic structures of two Sfp-type PPTases from Mycobacteria, PptT from *M. tuberculosis* and MuPPT from *M. ulcerans*, providing an atomic level comparison of the Sfp-type PPTase family. We also examined *in vitro* biochemical properties and tested a panel of known PPTase inhibitors to clarify these potential antibiotic targets for combating mycobacterial pathogens.

Experimentally, PptT was found to be insoluble upon heterologous expression in *E. coli*, as observed by Rottier et al.[25] Therefore, we began studying PptT as an N-terminal maltose binding protein (MBP) fusion. *In vitro* removal of the MBP domain via a thrombin protease cleavage site led to significant precipitation of PptT. Thermal stability experiments with the MBP-PptT fusion using a dye-binding thermal stability assay[26] led to modifications of purification buffer conditions to promote higher thermal stability. Although PptT has a calculated pI of 6.0, we found that maximum thermal stability was achieved between pH 5.5−5.8 (Supplementary Figure 2). Sodium chloride, glycerol, and calcium chloride further increased the stability of PptT (Supplementary Figure 3). These new buffer conditions enabled the expression and purification of a highly soluble C-terminal hexahistidine-tagged PptT construct (Supplementary Figure 4). PptT crystallized in the presence of its two cofactors CoA and Mg^{2+}. Due to low sequence homology between PptT and the Sfp-type PPTases previously characterized, experimental phasing data were obtained using selenomethionine (Se-Met) substituted PptT and single-wavelength anomalous diffraction (SAD) at 1.54 Å resolution. MuPPT shares 80% sequence identity with PptT and was thus subjected to identical purification strategies. The structure of MuPPT was phased by molecular replacement using the SAD-solved PptT structure. PptT and MuPPT were refined to final resolutions of 1.59 and 1.65 Å, respectively (Supplementary Table 1).

Both PptT and MuPPT possess pseudodimeric folds characteristic of Sfp-type PPTases (Figure 1a, Supplementary Figure 5a). The overall structures of these two PPTases resemble those of Sfp from *B. subtilis*[27] and HsPPT from *H. sapiens*,[16] despite 19% identity and 26% similarity to BsSfp, and 22% identity and 26% similarity to HsPPT (Supplementary Figure 5b−d, Supplementary Figure 6). Since BsSfp and HsPPT are relatively close phylogenetic relatives, while distant from PptT (Supplementary Figure 7), these new structures aid in understanding the structural diversity of Sfp-type PPTase 3D architectures at atomic resolution. CoAs are bound in the active sites located between the two pseudosymmetric halves of PptT and MuPPT. Despite the overall fold similarity between PptT, MuPPT, Sfp, and HsPPT, closer examination reveals several

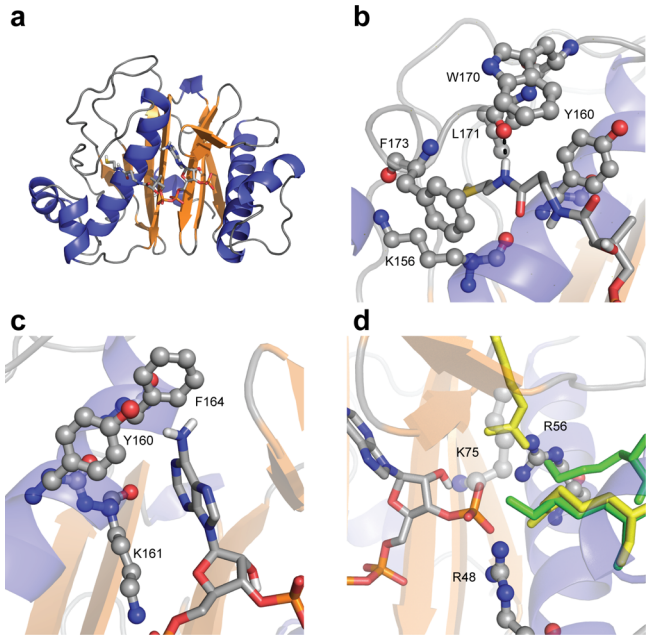

Figure 1. Crystal structure of PptT (PDB id 4QJK). β-Sheets are colored orange, and α-helices colored blue. Highlighted side chains are depicted as ball and stick models and colored by element. Ligands are depicted as stick models colored by element with polar hydrogens displayed. (a) Overall structure of PptT complexed with CoA, exhibiting a pseudodimeric structure characteristic of Sfp-type PPTases. (b) The interactions of the pantetheine binding tunnel with CoA are highlighted. The hydrogen bond between the backbone carbonyl oxygen of Leu171 and the amide hydrogen of pantetheine is highlighted with a black dotted line. (c) Depiction of the amino acids that form a deep hydrophobic pocket at the adenine binding site. The phosphopantetheine portion of CoA was omitted for clarity. (d) Coordination of the 3′-phosphate of CoA by Arg56 and Arg48. Lys75 of MuPPT was overlaid onto the PptT structure and depicted as slightly transparent. Depicted in yellow and green are the residues observed in HsPPT (PDB id 2C43) and Sfp (PDB id 1QR0), respectively, which coordinate the 3′-phosphate.

major differences in the active site architectures of the Mycobacterial PPTases.

The most striking difference involves the orientation of the pantetheine arm of CoA. In PptT and MuPPT, pantetheine extends into a deep hydrophobic pocket formed primarily by residues Tyr160, Leu171, Phe173, and Lys156 (Figure 1b). Trp170 serves as a "cap" above the entrance of this pocket. Furthermore, a key hydrogen bond between the backbone carbonyl of Leu171 and an amide nitrogen of the pantetheine arm is observed only in the Mycobacterium PPTases. Sequestration of the pantetheine arm is only partially observed in HsPPT and is absent in Sfp. The adenine base of CoA is buried in a deep, hydrophobic pocket (Figures 1c, 2a,b). This pocket is lined by Tyr160, Phe164, and Lys161. In both Sfp and HsPPT, the adenine base sits closer to the surface residing in a shallow pocket lined by fewer hydrophobic residues (Figure 2c,d). Residues that interact with the 3′-phosphate of CoA vary in identity and position along the backbone between the Mycobacterium PPTases, Sfp, and HsPPT (Figure 1d). PptT and MuPPT utilize Arg48 and Arg56, which are found in close proximity on the same α-helix. Lys75 may also serve as an electrostatic link, which is in close proximity to the 3′-phosphate in the MuPPT structure. In comparison, Sfp utilizes residues Lys28 and Lys31, and HsPPT utilizes Arg47 and

dx.doi.org/10.1021/cb500263p | *ACS Chem. Biol.* 2014, 9, 1939−1944

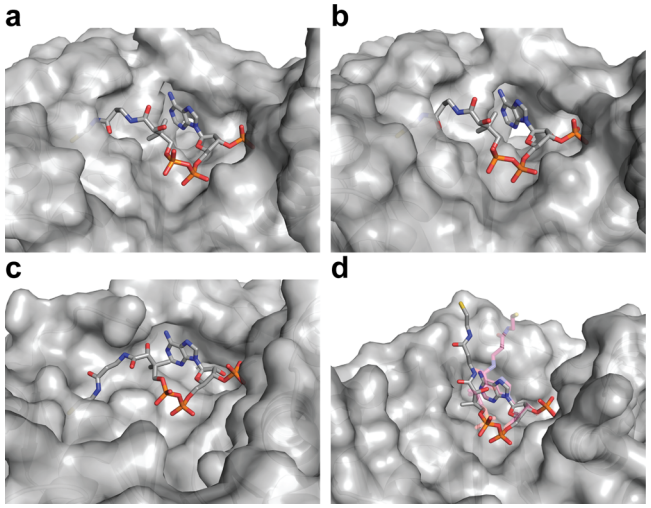

Figure 2. Surface representation of the CoA binding pocket of (a) PptT (PDB id 4QJK) (b) MuPPT (PDB id 4QJL), (c) HsPPT (PDB id 2C43), and (d) Sfp (PDB ids 4MRT, 1QR0). CoA is depicted as color-coded bonds on top of a gray protein-accessible surface. The CoA conformation observed in the 1QR0 Sfp structure is shown as semitransparent bonds, colored with purple carbons, and overlaid on the Sfp and CoA found in 4MRT.

Arg86. Sequence alignment of PptT, Sfp, and HsPPT reveals no apparent primary sequence conservation among these basic residues. These notable structural differences between the Mycobacterium PPTases and HsPPT should enable specific targeting of pathogenic Mycobacterial PPTases with PPTase inhibitors, a critical factor for the therapeutic index of any potential inhibitor candidates.

Although a majority of the active site residues of PptT and MuPPT form divergent interactions with CoA, the residues surrounding the Mg^{2+} ion and diphosphate moiety of CoA are similar to Sfp. Glu116 and Asp114 of PptT and MuPPT are positioned around the Mg^{2+} ion binding site. Lys161 and His93 both play a role in coordinating the α-phosphate of CoA during catalysis. All four of these catalytic residues are generally conserved throughout the Sfp-type PPTase family.[12] Glu157, which putatively coordinates the Mg^{2+} and deprotonates the Ser of the CP,[27] is rotated away from the Mg^{2+} center, and density for Mg^{2+} was not clearly observed in the structure of PptT. Due to the acidity of the crystallization conditions, it is possible that Glu157 is protonated, reducing its ability to effectively coordinate the Mg^{2+} ion. This would allow rotation of the carboxylate side chain away from the Mg^{2+} binding site. Similarly, in the structure of MuPPT, Glu157 is found in a different rotameric state (Supplementary Figure 8).

In activity studies, PptT efficiently labeled three recombinant CPs that represent FAS, NRPS, and PKS CP targets. FAS acyl carrier protein AcpP of *E. coli*, the vibriobactin peptidyl carrier protein VibB from *V. cholerae*, and mycocerosic acid synthase MAS from *M. tuberculosis* were labeled by PptT with a synthetic rhodamine-CoA analogue (Figure 3a).[28] MAS was used to assess activity against a native target, since it contains a CP domain that requires phosphopantetheinylation by an Sfp-type PPTase.[29] A previously described assay utilizing the blue pigment producing single module NRPS BpsA[30,31] was used to measure the relative activities of wild type PptT, MuPPT, and Sfp. The apparent k_{cat}/K_m (min^{-1} μM^{-1}) values of PptT and MuPPT were 0.26 ± 0.05 and 0.26 ± 0.06, respectively. Sfp activity was much lower, exhibiting a k_{cat}/K_m of 0.020 ± 0.004 (Figure 3b, Supplementary Table 2).

To better understand the catalytic mechanism of PptT, five active site mutants were generated and biochemically characterized (Supplementary Figure 9). On the basis of comparisons with the previously published crystal structure of Sfp,[27] Glu157, Asp114, Glu116, Arg48, and Arg56 of PptT were examined. Removal of the negative charge associated with the putative Mg^{2+} ligand/general base, E157Q, abolished phosphopantetheinylation activity. This activity loss was observed for the corresponding Glu to Gln mutation in both Sfp and HsPPT. The D114N mutation, which eliminates the negative charge of one of the putative Mg^{2+} ligands, also abolished phosphopantetheinylation activity of PptT. These results coincide with the corresponding mutation in both Sfp and HsPPT. A similar isosteric mutation of another Mg^{2+} coordinating residue, E116Q, reduced activity by 500-fold compared to wild type activity. The E109D mutation was made in Sfp, resulting in no measurable catalytic activity. In AcpS-type PPTases, the positions equivalent to Glu116 in PptT are nonpolar residues, specifically, Val in *M. tuberculosis* AcpS. Similarly, this acidic residue is sometimes absent in eukaryotic Sfp-type PPTases. For instance, HsPPT contains a Met at this position, suggesting that an acidic residue at this position is not absolutely essential for phosphopantetheinylation activity, while the acidic residues corresponding to Glu157 and Asp114 of PptT are absolutely conserved. Mutations chosen to disrupt 3′-phosphate binding, R48A and R56A, nonetheless retained activity at 20-fold and 100-fold reductions of wild type activity, respectively. Mutation of the basic residues that coordinate the 3′-phosphate in HsPPT significantly decreased the mutant enzymes' affinity for CoA, with a modest increase in catalytic

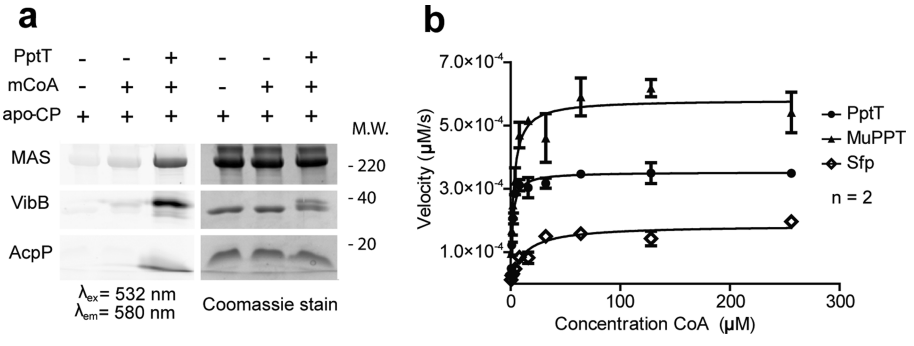

Figure 3. Activity of PPTases. (a) Gels depicting fluorescent labeling of the three carrier protein targets MAS, VibB, and AcpP with rhodamine CoA (mCoA) with PptT. (b) Michaelis–Menten fit of PptT (●), MuPPT (▲), and Sfp (◇) in the BpsA activity assay.

dx.doi.org/10.1021/cb500263p | *ACS Chem. Biol.* 2014, 9, 1939–1944

turnover. While important for CoA binding, Arg48 and Arg56 likely play very small roles in catalysis.

Sfp is known to retain cellular CoA throughout heterologous purification from *E. coli*.[21] Incubation of recombinant PptT with *apo*-AcpP was sufficient to generate the *holo*-AcpP product when monitored via a urea-PAGE gel shift assay, indicating that PptT also copurifies with tightly bound CoA (Supplementary Figure 10). To weaken the binding of this endogenously bound CoA to Sfp and PptT, calf intestinal alkaline phosphatase was used to remove the 3′-phosphate. Phosphatase-treated Sfp exhibited negligible conversion of *apo*-AcpP to *holo*-AcpP when compared to untreated enzyme, but PptT retained activity, indicating only partial removal of CoA. Since PptT mutants deficient in coordinating the 3′-phosphate are catalytically active, PptT might retain 3′-dephospho CoA throughout phosphatase treatment and utilize it as a substrate. The overall activity of Sfp and PptT was not affected by this treatment.

Partial removal of endogenous CoA from both Sfp and PptT enabled the measurement of the thermodynamic properties for CoA binding to the PPTases by isothermal titration calorimetry (ITC) (Supplementary Figure 11a). Sfp and PptT have dissociation constants (K_d's) of 3.4 ± 0.2 μM and 36 ± 13 nM, respectively. The calculated K_d for Sfp and CoA is comparable to previously reported values.[32] For Sfp, the enthalpy (ΔH, kcal mol^{-1}) and entropy ($T\Delta S$, kcal mol^{-1}) of binding are −12.5 ± 0.15 and −5.07 ± 0.38, respectively, and for PptT, −5.78 ± 0.08 and 4.14 ± 0.16, respectively. Both the enthalpic and entropic values contribute to the Gibbs free energy of binding of CoA to PptT. Combination of the hydrophobic adenine pocket, deep sequestration of the pantetheine arm, and 3′-phosphate coordination observed in the crystal structure might account for the enthalpically and entropically favored interaction between PptT and CoA. PptT and Sfp were also titrated with rhodamine CoA using ITC measurements. Sfp exhibited a K_d of 1.30 ± 0.19 μM, while a K_d between PptT and rhodamine CoA could not be calculated (Supplementary Figure 11b). While Sfp binds both CoA and rhodamine CoA with comparable affinity, PptT does not. These data suggest that while CoA is buried in the PptT active site, the rhodamine CoA analogue is incapable of adopting a similar high affinity interaction. The rhodamine CoA analogue may instead adopt a binding conformation similar to that of CoA in the structure of Sfp containing CoA and its CP substrate.[22] In this latter case, the pantetheine arm extends out of the binding pocket instead of into the pantetheine "tunnel" observed in the PptT crystal structure.

To date, only a small number of Sfp-type PPTase inhibitors have been identified.[33] We extended the analysis of these compounds to PptT utilizing a recently published fluorescence polarization (FP) assay that measures modification of a CP target with a synthetic fluorescent CoA analogue (Table 1).[34] The FP experiments with PptT were conducted using both VibB and MAS as CP targets. The IC_{50} values suggest that inhibition of PptT by these molecules is independent of the CP substrate. Inhibitors SCH202676, guanidinyl-naltrindole difluoroacetate, calmidazolium chloride, PD 404,182, and sanguinarine chloride exhibited the greatest inhibition of PptT activity while having no inhibitory activity against HsPPT.[34] Unlike the structure of PptT described here, HsPPT contains a C-terminal loop-helix motif that abuts the CoA binding pocket at the CP binding interface. These structural differences along with the selective inhibition of PptT bodes well for ongoing efforts of selective inhibitor design against these structurally distinct targets.

Table 1. Small Molecules Assayed against PptT for Inhibition in a Fluorescence Polarization Assay with Both VibB and MAS as the Target Carrier Protein

compound	IC_{50} (μM), PptT	
	MAS	VibB
CoA	1.1 ± 0.1	4.7 ± 0.4
3′,5′-PAP	1.6 ± 0.2	0.78 ± 0.20
2′-deoxy-3′,5′-PAP	7.4 ± 0.4	8.5 ± 1.0
mitoxantrone 2HCl	inactive	inactive
benserazide HCl	NC[a]	NC[a]
SCH-202676	0.5[b]	0.8[b]
Bay 11-7085	30 ± 4	NC
6-nitroso-benzopyrone	24 ± 2	17 ± 2
PD 404, 182	19 ± 1	7.1 ± 0.4
guanidinyl-naltrindole 2CF_3COOH	12 ± 1	19 ± 1
sanguinarine Cl	4.9 ± 0.2	22 ± 2
calmidazolium Cl	4.9 ± 0.4	2.0 ± 0.2
(−)-ephedrine hemisulfate	inactive	inactive

[a]Compounds displaying a reproducible but very small percent inhibition were not calculated (NC). Structures of each inhibitor can be found in Supplementary Table 4. [b]A large error was encountered while measuring the IC_{50} value.

In conclusion, we have characterized the Sfp-type PPTases PptT from *M. tuberculosis* and MuPPT from *M. ulcerans* both structurally and biochemically. Based on the structural and biochemical similarity between PptT and MuPPT and the structural differences with HsPPT, anti-mycobacterial drugs that target the Sfp-type PPTase might be generally applicable to other mycobacterial species including *M. leperae*, *M. bovis*, and *M. avium*, further increasing the value of PPTase inhibitors as antimicrobials.

METHODS

Thermofluor-Guided Buffer Optimization. MBP-PptT was diluted to 10 μM using 0.1 M solutions of 21 different buffers (Supplementary Figure 2) in a white 96-well plate. Sypro dye (Roche) was added to each well to a 10× final concentration. Each well held a total volume of 20 μL. The temperature was ramped from 25 to 85 °C at a rate of 0.06°/s using a Roche Lightcycler 480 (Roche). The negative first derivative of the raw fluorescence data was used to locate the melting curve inflection point to determine the midpoint melting temperatures (T_m). The buffers exhibiting the greatest increase in T_m for the PptT portion of the protein fusion were used to expand the screening in two additional dimensions varying the nature and concentration of salts and small molecule additives. Conditions providing the greatest T_m increases were combined and used for purification and storage of both PptT and MuPPT.

Additional Methods. For details on cloning and expression of protein, crystallization, activity and inhibition assays, ITC experiments, and CoA removal, please see Supporting Information.

ASSOCIATED CONTENT

Supporting Information

This material is available free of charge via the Internet at http://pubs.acs.org.

Accession Codes

The structures of PptT and MuPPT have been deposited under the PDB id codes 4QJK and 4QJL, respectively.

AUTHOR INFORMATION

Corresponding Authors

*E-mail: noel@salk.edu.

*E-mail: mburkart@ucsd.edu.

Notes

The authors declare no competing financial interest.

ACKNOWLEDGMENTS

We would like to thank G. Louie, M. Bowman, and J.-K. Weng for assistance with crystallographic procedures and D. Ackerley for the BpsA plasmid. This work was supported by NIH R01GM094924 and R01GM095970 (to M.D.B.), the National Science Foundation under Award EEC-0813570 (to J.P.N.), and the Howard Hughes Medical Institute (to J.P.N.).

REFERENCES

(1) Wilson, M. L. (2008) Reducing the global burden of mycobacterial infections: one more piece of the puzzle. *Am. J. Clin. Pathol. 130*, 849−852.

(2) Almeida Da Silva, P. E., and Palomino, J. C. (2011) Molecular basis and mechanisms of drug resistance in *Mycobacterium tuberculosis*: classical and new drugs. *J. Antimicrob. Chemother. 66*, 1417−1430.

(3) Russell, D. G., Barry, C. E., 3rd, and Flynn, J. L. (2010) Tuberculosis: what we don't know can, and does, hurt us. *Science 328*, 852−856.

(4) Wansbrough-Jones, M., and Phillips, R. (2006) Buruli ulcer: emerging from obscurity. *Lancet 367*, 1849−1858.

(5) Brennan, P. J. (2003) Structure, function, and biogenesis of the cell wall of *Mycobacterium tuberculosis*. *Tuberculosis 83*, 91−97.

(6) Neyrolles, O., and Guilhot, C. (2011) Recent advances in deciphering the contribution of *Mycobacterium tuberculosis* lipids to pathogenesis. *Tuberculosis 91*, 187−195.

(7) De Voss, J. J., Rutter, K., Schroeder, B. G., Su, H., Zhu, Y., and Barry, C. E., III (2000) The salicylate-derived mycobactin siderophores of *Mycobacterium tuberculosis* are essential for growth in macrophages. *Proc. Natl. Acad. Sci. U.S.A. 97*, 1252−1257.

(8) Reddy, P. V., Puri, R. V., Chauhan, P., Kar, R., Rohilla, A., Khera, A., and Tyagi, A. K. (2013) Disruption of mycobactin biosynthesis leads to attenuation of *Mycobacterium tuberculosis* for growth and virulence. *J. Infect. Dis. 208*, 1255−1265.

(9) George, K. M., Chatterjee, D., Gunawardana, G., Welty, D., Hayman, J., Lee, R., and Small, P. L. C. (1999) Mycolactone: A polyketide toxin from *Mycobacterium ulcerans* required for virulence. *Science 283*, 854−857.

(10) Mercer, A. C., and Burkart, M. D. (2007) The ubiquitous carrier protein—a window to metabolite biosynthesis. *Nat. Prod. Rep. 24*, 750−773.

(11) Gokhale, R. S., Saxena, P., Chopra, T., and Mohanty, D. (2007) Versatile polyketide enzymatic machinery for the biosynthesis of complex mycobacterial lipids. *Nat. Prod. Rep. 24*, 267−277.

(12) Beld, J., Sonnenschein, E. C., Vickery, C. R., Noel, J. P., and Burkart, M. D. (2014) The phosphopantetheinyl transferases: catalysis of a post-translational modification crucial for life. *Nat. Prod. Rep. 31*, 61.

(13) Lambalot, R. H., Gehring, A. M., Flugel, R. S., Zuber, P., LaCelle, M., Marahiel, M. A., Reid, R., Khosla, C., and Walsh, C. T. (1996) A new enzyme superfamily—the phosphopantetheinyl transferases. *Chem. Biol. 3*, 923−936.

(14) Elovson, J., and Vagelos, P. R. (1968) Acyl Carrier Protein: X. Acyl carrier protein synthetase. *J. Biol. Chem. 243*, 3603−3611.

(15) Lambalot, R. H., and Walsh, C. T. (1995) Cloning, overproduction, and characterization of the Escherichia coli holo-acyl carrier protein synthase. *J. Biol. Chem. 270*, 24658−24661.

(16) Bunkoczi, G., Pasta, S., Joshi, A., Wu, X., Kavanagh, K. L., Smith, S., and Oppermann, U. (2007) Mechanism and substrate recognition of human holo ACP synthase. *Chem. Biol. 14*, 1243−1253.

(17) Praphanphoj, V., Sacksteder, K. A., Gould, S. J., Thomas, G. H., and Geraghty, M. T. (2001) Identification of the alpha-aminoadipic semialdehyde dehydrogenase-phosphopantetheinyl transferase gene, the human ortholog of the yeast LYS5 gene. *Mol. Genet. Metab. 72*, 336−342.

(18) Donato, H., Krupenko, N. I., Tsybovsky, Y., and Krupenko, S. A. (2007) 10-Formyltetrahydrofolate dehydrogenase requires a 4′-phosphopantetheine prosthetic group for catalysis. *J. Biol. Chem. 282*, 34159−34166.

(19) Dym, O., Albeck, S., Peleg, Y., Schwarz, A., Shakked, Z., Burstein, Y., and Zimhony, O. (2009) Structure−function analysis of the acyl carrier protein Synthase (AcpS) from *Mycobacterium tuberculosis*. *J. Mol. Biol. 393*, 937−950.

(20) Gokulan, K., Aggarwal, A., Shipman, L., Besra, G. S., and Sacchettini, J. C. (2011) *Mycobacterium tuberculosis* acyl carrier protein synthase adopts two different pH-dependent structural conformations. *Acta Crystallogr., Sect. D: Biol. Crystallogr. 67*, 657−669.

(21) Mofid, M. R., Marahiel, M. A., Ficner, R., and Reuter, K. (1999) Crystallization and preliminary crystallographic studies of Sfp: a phosphopantetheinyl transferase of modular peptide synthetases. *Acta Crystallogr., Sect. D: Biol. Crystallogr. 55*, 1098−1100.

(22) Tufar, P., Rahighi, S., Kraas, F. I., Kirchner, D. K., Löhr, F., Henrich, E., Köpke, J., Dikic, I., Güntert, P., Marahiel, M. A., and Dötsch, V. (2014) Crystal structure of a PCP/Sfp complex reveals the structural basis for carrier protein posttranslational modification. *Chem. Biol. 21*, 552−562.

(23) Chalut, C., Botella, L., de Sousa-D'Auria, C., Houssin, C., and Guilhot, C. (2006) The nonredundant roles of two 4′-phosphopantetheinyl transferases in vital processes of Mycobacteria. *Proc. Natl. Acad. Sci. U.S.A. 103*, 8511−8516.

(24) Leblanc, C., Prudhomme, T., Tabouret, G., Ray, A., Burbaud, S., Cabantous, S., Mourey, L., Guilhot, C., and Chalut, C. (2012) 4′-Phosphopantetheinyl transferase PptT, a new drug target required for *Mycobacterium tuberculosis* growth and persistence *in vivo*. *PLoS Pathog. 8*, e1003097.

(25) Rottier, K., Faille, A., Prudhomme, T., Leblanc, C., Chalut, C., Cabantous, S., Guilhot, C., Mourey, L., and Pedelacq, J.-D. (2013) Detection of soluble co-factor dependent protein expression *in vivo*: Application to the 4′-phosphopantetheinyl transferase PptT from *Mycobacterium tuberculosis*. *J. Struct. Biol. 183*, 320−328.

(26) Ericsson, U. B., Hallberg, B. M., DeTitta, G. T., Dekker, N., and Nordlund, P. (2006) Thermofluor-based high-throughput stability optimization of proteins for structural studies. *Anal. Biochem. 357*, 289−298.

(27) Reuter, K., Mofid, M. R., Marahiel, M. A., and Ficner, R. (1999) Crystal structure of the surfactin synthetase-activating enzyme sfp: a prototype of the 4′-phosphopantetheinyl transferase superfamily. *EMBO J. 18*, 6823−6831.

(28) Foley, T. L., and Burkart, M. D. (2009) A homogeneous resonance energy transfer assay for phosphopantetheinyl transferase. *Anal. Biochem. 394*, 39−47.

(29) Rainwater, D. L., and Kolattukudy, P. E. (1985) Fatty acid biosynthesis in *Mycobacterium tuberculosis* var. *bovis Bacillus Calmette-Guérin*. Purification and characterization of a novel fatty acid synthase, mycocerosic acid synthase, which elongates n-fatty acyl-CoA with methylmalonyl-CoA. *J. Biol. Chem. 260*, 616−623.

(30) Takahashi, H., Kumagai, T., Kitani, K., Mori, M., Matoba, Y., and Sugiyama, M. (2007) Cloning and characterization of a Streptomyces single module type non-ribosomal peptide synthetase catalyzing a blue pigment synthesis. *J. Biol. Chem. 282*, 9073−9081.

(31) Owen, J. G., Copp, J. N., and Ackerley, D. F. (2011) Rapid and flexible biochemical assays for evaluating 4′-phosphopantetheinyl transferase activity. *Biochem. J. 436*, 709−717.

(32) Duckworth, B. P., and Aldrich, C. C. (2010) Development of a high-throughput fluorescence polarization assay for the discovery of phosphopantetheinyl transferase inhibitors. *Anal. Biochem. 403*, 13−19.

(33) Yasgar, A., Foley, T. L., Jadhav, A., Inglese, J., Burkart, M. D., and Simeonov, A. (2010) A strategy to discover inhibitors of *Bacillus*

subtilis surfactin-type phosphopantetheinyl transferase. *Mol. Biosyst. 6*, 365−375.
(34) Kosa, N. M., Foley, T. L., and Burkart, M. D. (2013) Fluorescent techniques for discovery and characterization of phosphopantetheinyl transferase inhibitors. *J. Antibiot. (Tokyo) 67*, 113−120.